ADVANCED MATERIALS
www.advmat.de

Buckle-Barrel Correspondence Based on Topological Polarization Conversion in Mechanical Metamaterials

*Jingyi Zhang, Jingran Liu, Anton Souslov, María Teresa Pérez Prado, Javier Segurado, Maciej Haranczyk, and Johan Christensen**

Harnessing instabilities in architected lattices and metamaterials allows for controlled nonlinear deformations, enabling desired mechanical functions like shape morphing and energy absorption. By precisely tailoring instabilities such as buckling into the structure, deformations become a powerful instrument rather than a failure mode, offering new possibilities for predictable responses to mechanical loads. Inspired by the bulk-boundary correspondence in condensed matter physics, an analogous relationship is explored in metamaterials, where the underlying topology dictates whether the structure under load buckles or barrels. The underlying mechanism that originates from a polarization conversion in the elementary beam network is discussed. Moreover, these predictions, which can be extended to more complex topologies and higher dimensions, showcase that a mode inversion process governs both global deformations and the orientation of localized shear strains within the bulk. It is anticipated that the buckle-barrel correspondence can be extended to non-Hookean materials, paving the way for predicting the onset and evolution of true failure.

1. Introduction

Topological band theory is a framework in condensed matter physics that describes how the electronic properties of materials are influenced by their underlying symmetries. This theory examines the energy bands, which typically determine whether a material is conducting or insulating, while also considering the role of symmetry and robustness against perturbations. The associated properties are topologically steadfast and remain unchanged, as illustrated by the classical example of a doughnut and a coffee mug, where one can be reshaped into the other without altering their fundamental structure. A key insight from this theory is the concept of bulk-boundary correspondence, which explains how some materials, due to their topological properties, can conduct electricity on their surfaces or edges while their bulk interior remains insulating.[1,2]

Metamaterials have capitalized on this topological notion, by adding the components of symmetry to defect-resilient guiding of sound, light, and vibrations. In this arena, the bulk-boundary correspondence also plays a vital role, in that the topology, determines whether waves trivially enter the lattice-bulk or remain protected in the form of surface confining states (modes). Moreover, this approach has been leveraged to play a keyrole in up and coming systems and devices for robust optical communication, quantum computing and information, as well as topological lasers and sasers.[3–7] Focusing on topological mechanics comprising Maxwell's and isostatic lattices, which are systems on the verge of mechanical instability where the number of constraints is balanced with the degrees of freedom, their tunable flexibility and rigidity make them ideal candidates for studying mechanical states localized at boundaries. Specifically, in isostatic lattices, where the structure is exactly constrained, the inherent isostaticity allows for the definition of an underlying topological invariant (polarization), much like topological insulators in condensed matter physics.[8–12] Beyond these constrained rigid motions, topology also plays a key role in a wide range of unstable solid mechanical lattices. Metamaterials made from lattices of slender beams exhibit unique properties due to mechanical instabilities, as these beams primarily deform through bending and can buckle under compressive loads, depending on their arrangement. These instabilities are typically considered failures in traditional materials, but in metamaterials, they are harnessed to enable novel mechanical behaviors.[13–15] E.g., metamaterials have been designed with meticulously engineered instabilities, whose holey shapes determine the optimal effective compaction.[16,17] Also, hinge-connected rigid quadrilateral metamaterials have both shown nonuniform soft dilatation conformal and kirigami macroscale deformations.[18,19] These carefully engineered instabilities offer applications in adaptive structures and soft robotics, fast actuation due to snap-through instabilities, as well as energy absorption, shape morphing, and tunable mechanical responses.[20–24]

J. Zhang, J. Liu, M. T. P. Prado, J. Segurado, M. Haranczyk, J. Christensen
IMDEA Materials Institute
Calle Eric Kandel, 2, Getafe, Madrid 28906, Spain
E-mail: johan.christensen@imdea.org
A. Souslov
TCM Group, Cavendish Laboratory
JJ Thomson Avenue, Cambridge CB3 0HE, UK
J. Segurado
Department of Materials Science
Universidad Politécnica de Madrid, E.T.S. de Ingenieros de Caminos Canales y Puertos, 28040 Madrid, Spain

The ORCID identification number(s) for the author(s) of this article can be found under https://doi.org/10.1002/adma.202415962

[Correction added on March 1, 2025, after first online publication: Author name M.H. in the author byline was corrected.]

DOI: 10.1002/adma.202415962

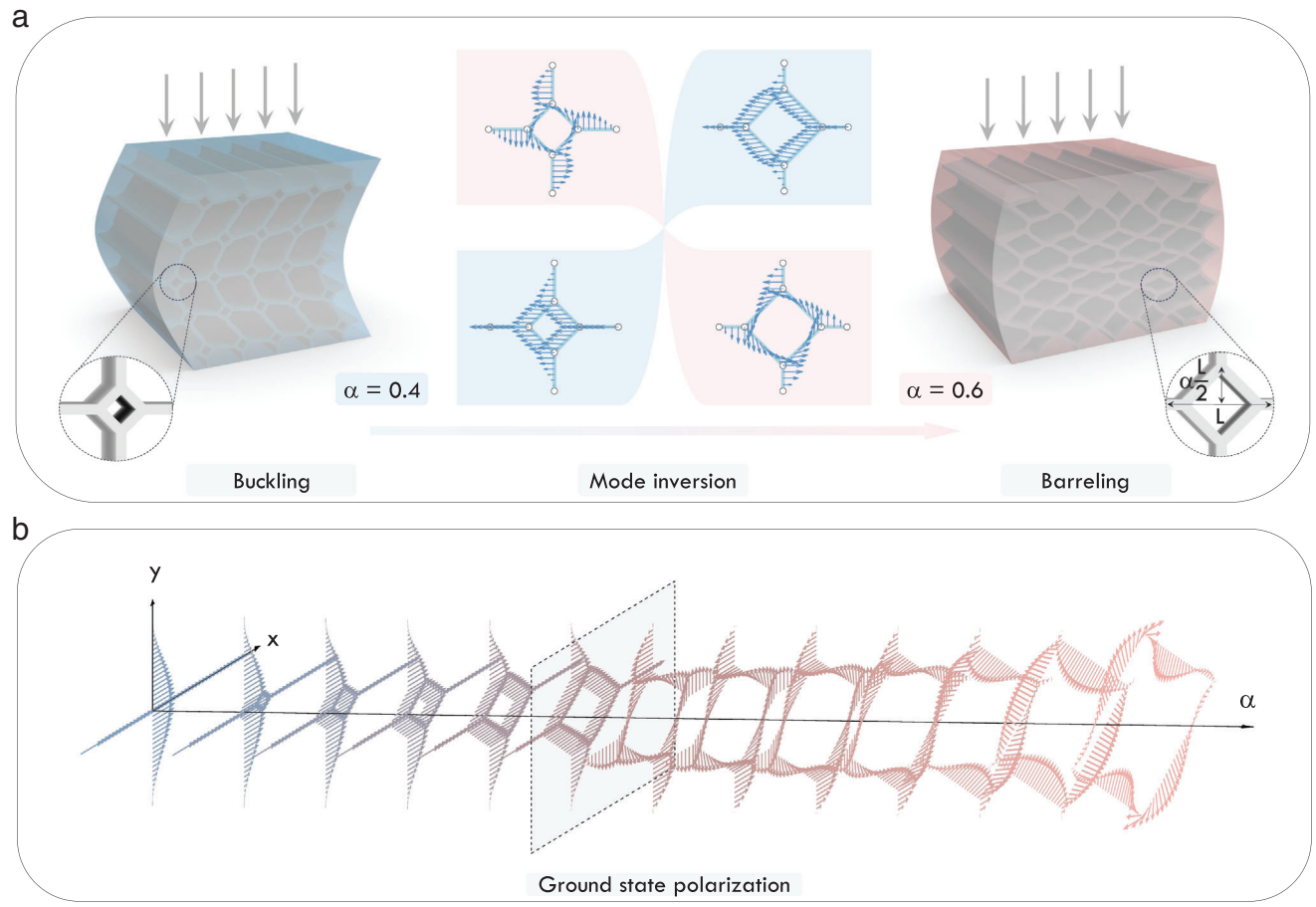

Figure 1. The buckle-barrel correspondence. a) The topology of a mechanical metamaterial whose constituents are slender beams is controlled through a single structural factor α, where L is the length of the square unit cell. Thus, under uniaxial compression, both local and global instabilities are governed by this factor that scales the size of the central square element. It is seen, in dependence of α, that the finite specimen undergoes a transition from global buckling (blue) to symmetrical barreling (red). These global deformations are triggered by the lowest energy i.e., the ground state of the inverting buckling modes that collectively, depending on the topology, either slide (shear, blue) or rotate (red). b) The polarization of the ground state consists of in-plane (xy) buckling, as depicted by the morphing of elementary metamaterial units. In the direction of the third axis, along which α varies, the sliding of the unit cell, composed of eight beams, transitions into rotational motion across the gray plane, indicating the threshold of the polarization transition.

In this contribution, while focusing on hyperelastic base materials, we examine the role of symmetry in relation to global deformations of metamaterial specimens. Inspired by non-Hookean responses that lead to a class of failure mechanisms, we explore how topology influences the onset of shear bands, which, in elasto-plastic materials, are localized zones of intense deformation that often precede failure. In contrast, hyperelastic materials such as rubbers, biological tissues, and other highly deformable substances return to their original shape once the applied stress is removed and do not crack or yield. We develop a semi-numerical method to rationally classify buckling modes, both at the local and global levels, in 2D structured metamaterials composed of connected slender Euler–Bernoulli beams. We discuss how this 2D artificial system can either buckle or barrel in a controlled manner, causing the entire structure under load to compress according to the rationally designed local topology. Qualitatively reminiscent of band inversion in topological insulators where conduction and valence bands swap roles due to symmetry-related effects, the inversion among fundamental buckling modes through a structural factor, gives rise to a global deformation transition driven by local polarization conversion. Thus, letting the topology trigger a transition from local shearing (sliding) to rotation, significantly alters localized strain fields and determines how these reversible global deformations of finite structures unfold. We foresee that the reported topological buckle-barrel correspondence may potentially establish fundamental principles for future shape-morphing materials and deployable structures, such as those used in space settlement or medical devices. Furthermore, we predict that extending our concept to truly non-Hookean materials may enable mechanical failure responses by design.

2. Results and Discussion

2.1. Buckle-Barrel correspondence

Beyond isostaticity or rigid elements, we take the approach resting on Euler-Bernoulli beam theory in the exploration of the

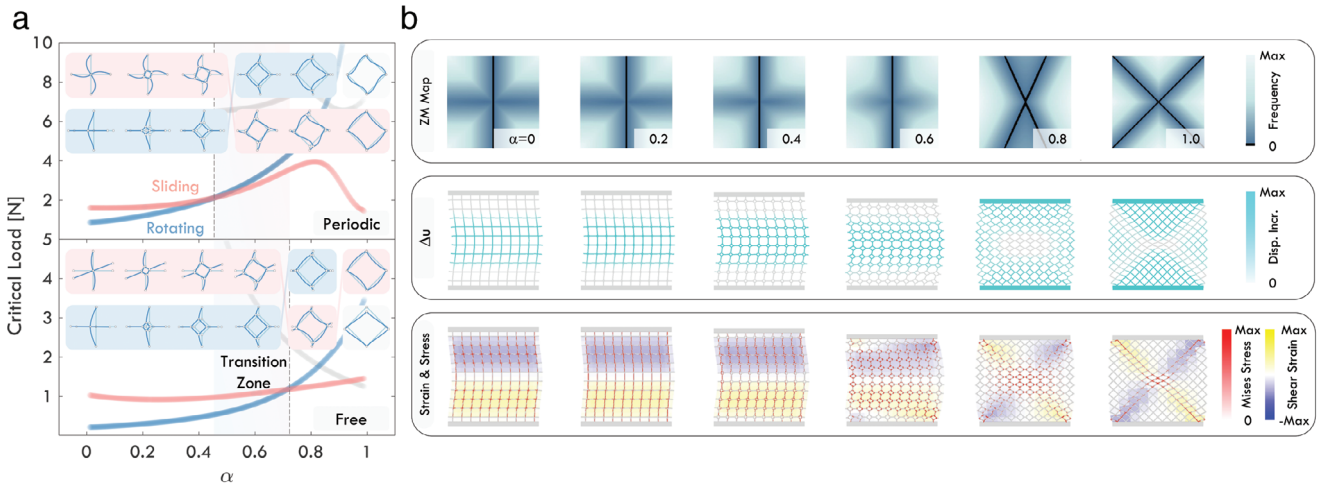

Figure 2. Micro-macro instabilities for a metamaterial with centrosymmetric units. a) Critical loads and corresponding instability polarizations of the unit cell as a function of the structural factor α using both periodic and free boundary conditions. The polarizations are grouped by colors and the gray transition zone originates from the ground state inversion points (dashed lines) at their respective boundary conditions. b) Zero mode maps obtained from a quasi-static Bloch-wave analysis vs. α, where the frequency approaches zero near the Γ point within the first Brillioin zone, which indicates a directional instability in reciprocal space. $\Delta u(\alpha)$ represents an incremental displacements at the onset of structural instability. Von-Mises stress and shear strain computations are superimposed on the same deformed configurations, indicating the localization of stress and strain when instabilities have set in.

buckle-barrel correspondence and its fundamental solid mechanical consequences. In doing so, each node of a single beam element has three degrees of freedom: translation displacements in both the vertical (perpendicular deflection) and axial directions (stretching or compression), as well as rotation due to bending moments, see Supporting Information for details. In conventional materials, the chemistry and its underlying atomistic topology determines its mechanical capabilities like the way it deforms under, e.g., an uniaxially applied force as rendered in **Figure 1a**. In here, as illustrated, we consider a mechanical metamaterial that is composed of a hyperelastic base material, i.e., no hysteresis and a pronounced linear regime. Its unit cell is composed of a network of eight slender beams, forming a topology of tilted squares and octagons, reminiscent of Haeckelite or T-graphene.[25,26] The backbone of the buckle-barrel correspondence that radically dictates the global mechanics is based on a local polarization conversation of the slender beam units. While either buckling or barreling of the metamaterial specimen is associated with low energy deformation of individual beams, i.e., their fundamental beam mode, the collective behaviour of all beams presents a richer picture. As shown in Figure 1a, while a structural factor α (defined over the range [0, 1]) that controls the size of the central square with respect to the unit cell (of length L) alters the topology, an inversion among the modes of the beams-unit takes place simultaneously. In concrete, sliding (shearing) unstable buckling energetically swaps place with the rotating unstable counterpart. In other words, global low-energy buckling at the ground state is associated with local sliding. As the topology changes, as illustrated, local rotation within the unit cell causes overall barreling during compression. Later, we discuss how this mode inversion leads to shifts in instability, i.e., a change in directionality of the associated zero modes (ZMs) in reciprocal space. Figure 1b illustrates the associated in-plane buckling of the unit cell as a function of the structural factor α across the inversion point, represented here as a gray plane. The conversion of the ground state polarization depicts the mechanism that transforms the global unstable deformation from buckling to barreling. In what follows, numerical and experimental discussions will paint a clear picture of how the underlying lattice topology of unstable metamaterials controls global deformation and bulk strain localization when subject to a generic uniaxial load.

2.2. From Micro to Macro Instabilities

In order to ascribe a spatial orientation to the instability of the 2D metamaterial and also to give meaning to global deformations, we investigate the ZMs and eigenvalues to rationally characterize the buckling modes including their polarization at the critical loads. For this, our starting point is the governing equation for a network of periodic Euler–Bernoulli beams:[27]

$$\mathbf{Q}^{\dagger}(\mathbf{k})(\tilde{\mathbf{K}}_e - \mathbf{P} \otimes \tilde{\mathbf{K}}_g)\mathbf{Q}(\mathbf{k})\tilde{\mathbf{u}} + \omega^2 \mathbf{Q}^{\dagger}(\mathbf{k})\tilde{\mathbf{M}}\mathbf{Q}(\mathbf{k})\tilde{\mathbf{u}} = \mathbf{0} \tag{1}$$

where $\mathbf{Q}(\mathbf{k})$, $\tilde{\mathbf{K}}_e$, $\mathbf{P}$, $\tilde{\mathbf{K}}_g$, ω, $\tilde{\mathbf{M}}$ and $\tilde{\mathbf{u}}$ represent the Bloch matrix, assembled elastic stiffness matrix, axial force distribution, assembled geometric matrix, eigenfrequency, assembled mass matrix and displacement vector, respectively. The symbol $\otimes$ denotes the assignment of the components of the axial force distribution $\mathbf{P}$ to the corresponding beams (see Supporting Information for details). For static problems, the inertial term must be removed, leading to a generalized eigenvalue problem in terms of $\mathbf{P}$:

$$\mathbf{Q}^{\dagger}(\mathbf{k})\tilde{\mathbf{K}}_e\mathbf{Q}(\mathbf{k})\tilde{\mathbf{u}} - \mathbf{P} \otimes \mathbf{Q}^{\dagger}\tilde{\mathbf{K}}_g\mathbf{Q}(\mathbf{k})\tilde{\mathbf{u}} = \mathbf{0} \tag{2}$$

To characterize the instability in the unit cell and the finite structure, we determine both the triggering critical load and the corresponding mode, which describes the elementary deformation.

The critical load **P** that induces instability is determined by solving Equation (2) where the lowest non-trivial eigenvalue of this equation defines the onset of instability, from which the corresponding displacement mode can also be identified. To accurately capture the correspondence between the behaviour of the unit cell (micro) and the overall finite structure (macro), it is essential to account for the effect of a set of mixed boundary conditions. Deep within the bulk of the metamaterial, periodic boundary conditions provides a good approximation, while for the units near the termination, free boundary condition is more appropriate. If we vary the topology through α and solve Equation (2) at the Γ point considering both types of boundary conditions separately, we obtain the respective critical loads of different orders, i.e., the axial forces that trigger the instability and the corresponding deformation modes, as shown in **Figure 2**a. From the two lowest order instability modes [red and blue bands, with respective mode profiles, both obtained from Equation (2)] it is seen that a transition zone is formed whose edges mark the mode inversion points with respect to the named boundary conditions. Across this zone, as discussion in Figure 1, the corresponding ground state polarization converts. More details and discussions can be found in the Supplementary Materials. Specifically, mode inversion occurs around $\alpha = 0.45$ for periodic and around $\alpha = 0.70$ for free boundary conditions, across which, the eigen-polarization transitions from sliding to rotating. By solving Equation (2), specifically, in the vicinity of the Γ point, i.e., in the quasi-static limit, we substitute the eigenvalues **P** back into Equation (1) to account for inertia to look for the ZMs in terms of ω. The zero-mode maps, representing the lowest dispersion around Γ, as shown in Figure 2b, serve to predict global deformation of the finite metamaterial specimen. Determining the ZM instabilities in reciprocal space, mathematically speaking, represent a directional (in momentum space) loss of positive definiteness of the stiffness matrix, consequently, resulting in a non-trivial null space of the stiffness matrix. Hence, apart from the trivial solution exactly at the Γ point, ZM contours display the direction of a single wavefront of infinite wavelength.

E.g., up until approximately $\alpha = 0.40$, the ZM maps depict perfect lines along which $k_x = 0$, indicating a single non-propagating quasi-static wavefront seemingly traversing along the vertical direction. From a solid mechanical point of view, using finite element simulations, In Figure 2b we also illustrate the incremental displacement Δu at the onset of instability, as well as the shear strain and stress fields (details can be found in the Supporting Information). The shear strain and Von-Mises stress fields reveal strong localization, reminiscent of shear bands, with orientations consistent with the directionalities observed in the ZM maps. Minor discrepancies are attributed to finite size effects. Ultimately, the transition from global buckling to barreling in the metamaterial specimens, driven by a sliding-to-rotating polarization conversion of the mechanical ground state, is accompanied by corresponding changes in the ZM orientation in reciprocal space. The transition from sliding to rotating can be described using a *buckling order* that is reminiscent of, yet distinct from, the Chern number used to characterize topological insulators:

$$C = \sum_{n=1}^{N} \int_{0}^{L_n} \kappa(l)\, dl \tag{3}$$

where N is the total number of beams in the unit cell, L_n is the length of the nth beam, and $\kappa(l)$ is the curvature of the beam. The buckling order captures the cumulative curvature integrated over all beams in the structure. In the sliding mode, the curvature integral is zero, yielding $C = 0$. In contrast, in the rotational mode, the curvature integrates to a non-zero value, resulting in $C \neq 0$. This formulation effectively distinguishes between the two deformation mechanisms and provides a quantitative means to describe the smooth transition observed in Figure 2a (see Supporting Information).

We now add a twist to the centrosymmetric structure to acquire larger degree of strain localization within the bulk of loaded metamaterials (see Supporting Information for a direct comparison). Taking the same approaches that were discussed earlier and comparing the critical loads for the centrosymmetry and the chiral units, we immediately observe a narrowing of the transition zone that is followed by a shift toward larger values of the structural factor α. The physical mechanism remains the same, i.e., a conversion from sliding to rotating. However, adding a twist to the units has a more dramatic effect when comparing the axes of the directional ZM maps with the localized bands of shearing instabilities. From the ZM contours vs. α, we predict a new attribute associated with the buckle-barrel correspondence. As shown in **Figure 3**b, changing the structural factor, within the sliding phase, generates a clockwise rotation of the ZM line (deep black), which gives rise to incremental displacements $\Delta u(\alpha)$ and shear strain bands that follow the direction along which the ZM lines point. In the rotating phase, again, two ZM lines cross, which implies barreling of the finite configuration with oppositely shearing instability bands (yellow and blue) that symmetrically cross. Note that for both the centrosymmetric and chiral units, we derive the effective Poisson's ratio, whose respective rapid increase (centrosymmetric) and sign change (chiral) coincide with the polarization conversion. Furthermore, we also discussed a star-shaped configuration whose topology, controlled by a single parameter, also leads to versatile mechanical instabilities (see Supporting Information).

2.3. Experimental Verification

The experimental samples are additively manufactured with TPU 95A as the base material. Additional simulations confirmed the sufficiency in choosing 10-by-10 unit cells (more details in the Supporting Information). During printing, we added upper and lower buffer layers that were glued to the loading disk of the uniaxial testing machine to avoid global horizontal shearing, as seen in **Figure 4**. The compression was performed at the same speed as in the computations (0.01[mm/s]). In Figure 4a (Figure 4b) we compare the stress-strain curves both from finite element prediction and measurements for the centrosymmetric (chiral) topological metamaterial. The results indicate that the topology of the unit cell affects both the linear and nonlinear responses of the finite structures. In both cases, it is seen that varying the structural factor α generates a smearing out of the initial buckling instability. Although, there is a general agreeing trend among measured and simulated data, the discrepancy around the stress peak of global instability originates from inherent viscosity that comes into effect at fast loading speeds. As discussed in the Supporting

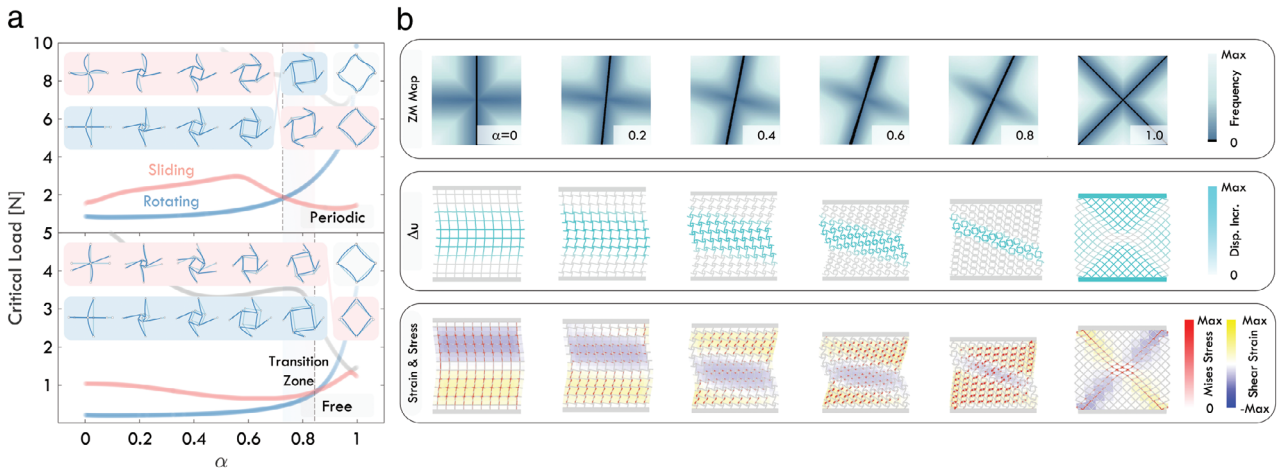

Figure 3. Micro-macro instabilities for a metamaterial with chiral units. a) Critical loads and corresponding instability polarizations of the unit cell as a function of the structural factor α using both periodic and free boundary conditions. The polarizations are grouped by colors and the gray transition zone originates from the ground state inversion points (dashed lines) at their respective boundary conditions. b) Zero mode maps obtained from a quasi-static Bloch-wave analysis versus α, where the frequency approaches zero near the Γ point within the first Brillioin zone, which indicates a directional instability in reciprocal space. $\Delta u(\alpha)$ represents an incremental displacements at the onset of structural instability. Von-Mises stress and shear strain computations are superimposed on the same deformed configurations, indicating the localization of stress and strain when instabilities have set in.

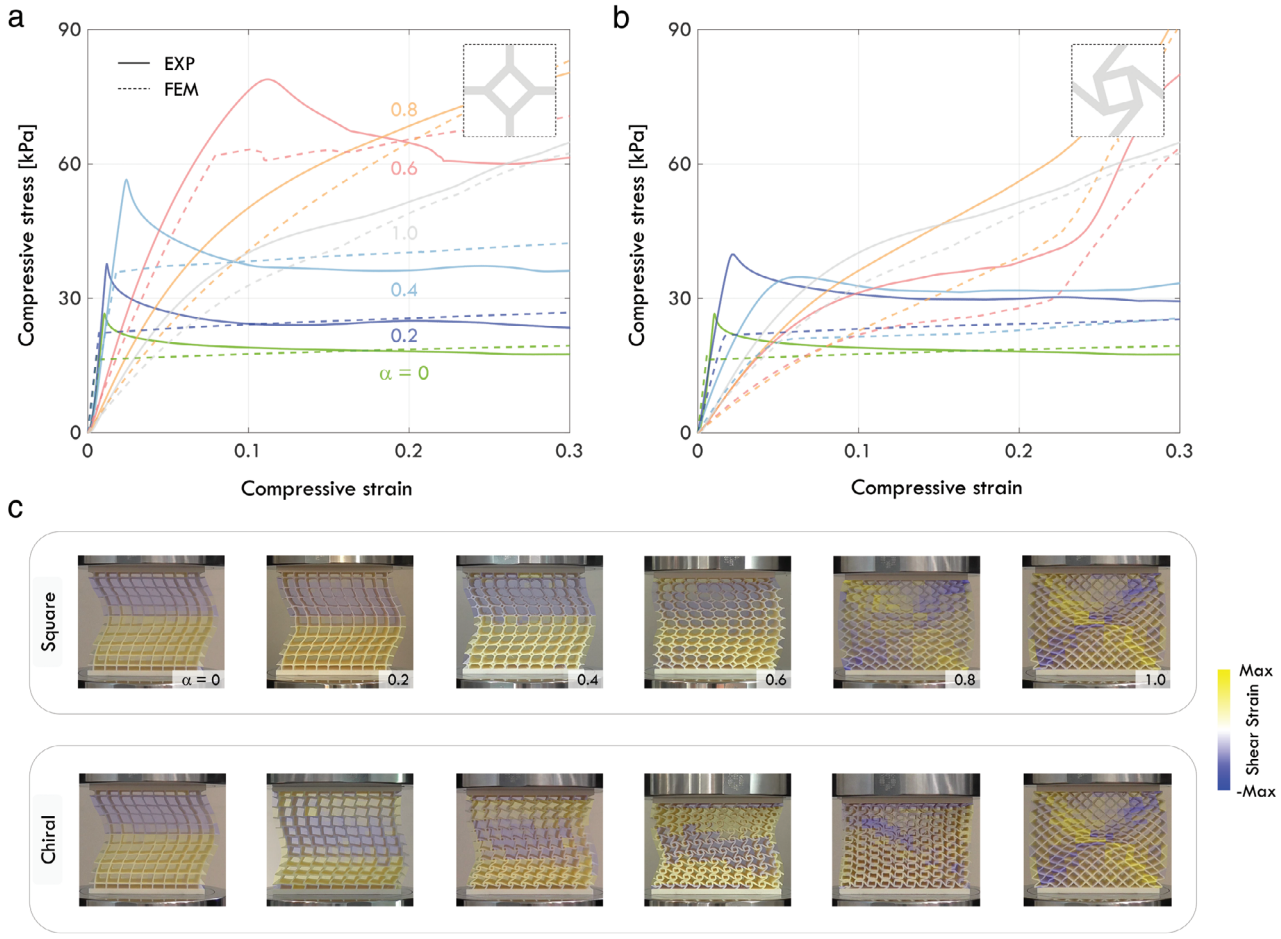

Figure 4. Stress versus strain and mapped shear strains. Experimental compressive stress-strain curves for different structural factors α for metamaterials with, a) centrosymmetric (square) and, b) chiral unit cells. We compare finite element computations (dashed) with measured data (full lines). c) Uniaxial loading experiments for various topologies with superimposed shear strains.

Information, lowering the compression speed to satisfy quasi-static conditions diminishes the adverse effect of damping due to energy dissipation through internal friction. Thus, increasing the time of uniaxial compression lowers the unstable stress from a linear onset toward plateauing levels. During testing, a digital camera records the compression out of which frames are chosen to still the moments of instabilities as shown in Figure 4c. From those frames, we spatially collect data points by dividing the cells into regimes (see Supporting Information), used to map the shear strain as shown atop of the compressed samples. First, we observe experimentally how the structural factor dictates the transition from global buckling to barelling. This proves that while materials do have an effect, the topology in as much is capable to let micro-instabilities dictate global deformations. Next, the shearing strain fields in the centrosymmetric (square) metamaterial sample display great agreement with simulations discussed in Figure 2. Moreover, the unstable shear bands discussed in Figure 3 concerning the chiral counterpart is very convincingly verified in the lower panel of Figure 4, in which its axes, in accordance to the ZM maps, rotate clockwise, across the phases pertaining to the buckle-barrel correspondence.

3. Conclusion

We discussed, based on a semi-numerical treatment and experiments, how the local micro-topology in structured, unstable beam-based metamaterials dictates global mechanical behaviour. What we coined the buckle-barrel correspondence describes the correlation between local polarizations transitions and macro-scale deformations. We found that local sliding (or rotating) of the elementary beam network gives rise to global buckling (or barreling) of the finite metamaterial sample under external load. Interestingly, the orientation of highly concentrated shear strain instabilities also aligns with theoretical predictions from reciprocal space analysis. We foresee that our findings could potentially serve as a new paradigm, broadening the geometrical design parameters in future shape-morphing and hierarchical mechanical metamaterials for deployable systems used for space and medical applications. Generally speaking, we believe that notions inspired by topological states of matter, such as the ubiquitous bulk-boundary correspondence, hold great potential to foster new interdisciplinary opportunities in areas such as structural engineering and material science when applied to structured metamaterials. Lastly, we note that there is an imminent opportunity, inspired by origami metamaterials, to use folding strategies to broaden the landscape of advanced topological deformations.[28–30] Additionally, richer tunability for inducing topological changes could be achieved through external biases using magnetic or thermal fields.

Supporting Information

Supporting Information is available from the Wiley Online Library or from the author.

Acknowledgements

The authors would like to express their gratitude to José Luis Jimenez and Vanesa Martinez for their assistance with the experimental efforts. The authors acknowledge the financial support from the European Union's NextGenerationEU/PRTR funds and M-ERA.NET's PORMETALOMICS project supported by MCIN/AEI/10.13039/501100011033, and the support from the Spanish Ministry of Science under grant PID2023-150075OB-I00.

Conflict of Interest

The authors declare no conflict of interest.

Data Availability Statement

The data that support the findings of this study are available in the Supporting Information of this article.

Keywords

mechanical metamaterials, topological metamaterials

Received: October 18, 2024
Revised: January 24, 2025
Published online: February 26, 2025

[1] M. Z. Hasan, C. L. Kane, *1Rev. Mod. Phys.* **2010**, *82*, 3045.
[2] B. A. Bernevig, T. L. Hughes, *Topological Insulators and Superconductors*, Princeton University Press, Princeton, NJ, **2013**.
[3] T. Ozawa, H. M. Price, A. Amo, N. Goldman, M. Hafezi, L. Lu, M. C. Rechtsman, D. Schuster, J. Simon, O. Zilberberg, I. Carusotto, *Rev. Mod. Phys.* **2019**, *91*, 015006.
[4] X. Zhang, F. Zangeneh-Nejad, Z.-G. Chen, M.-H. Lu, J. Christensen, *Nature* **2023**, *618*, 687.
[5] M. Aghaee, A. Akkala, Z. Alam, R. Ali, A. A. Ramirez, M. Andrzejczuk, A. E. Antipov, P. Aseev, M. Astafev, B. Bauer, J. Becker, S. Boddapati, F. Boekhout, J. Bommer, E. B. Hansen, T. Bosma, L. Bourdet, S. Boutin, P. Caroff, L. Casparis, M. Cassidy, A. W. Christensen, N. Clay, W. S. Cole, F. Corsetti, A. Cui, P. Dalampiras, A. Dokania, G. de Lange, M. de Moor, *Phys. Rev. B* **2023**, *107*, 245423.
[6] Y. Zeng, U. Chattopadhyay, B. Zhu, B. Qiang, J. Li, Y. Jin, L. Li, A. G. Davies, E. H. Linfield, B. Zhang, Y. Chong, Q. J. Wang, *Nature* **2020**, *578*, 246.
[7] B. Hu, Z. Zhang, H. Zhang, L. Zheng, W. Xiong, Z. Yue, X. Wang, J. Xu, Y. Cheng, X. Liu, J. Christensen, *Nature* **2021**, *597*, 655.
[8] K. Sun, A. Souslov, X. Mao, T. C. Lubensky, *Proc. Natl. Acad. Sci. USA* **2012**, *109*, 12369.
[9] T. Lubensky, C. Kane, X. Mao, A. Souslov, K. Sun, *Rep. Prog. Phys.* **2015**, *78*, 073901.
[10] X. Mao, T. C. Lubensky, *Annu. Rev. Condens. Matter Phys.* **2018**, *9*, 413.
[11] H. Kedia, A. Souslov, D. Z. Rocklin, *Phys. Rev. B* **2021**, *103*, L060104.
[12] Z. Tang, F. Ma, F. Li, Y. Yao, D. Zhou, *Phys. Rev. Lett.* **2024**, *133*, 106101.
[13] M. S. Anderson, *AIAA journal* **1981**, *19*, 782.
[14] R. G. Hutchinson, N. A. Fleck, *J. Mech. Phys. Solids* **2006**, *54*, 756.
[15] K. Bertoldi, M. C. Boyce, *Phys. Rev. B–Condensed Matter and Materials Physics* **2008**, *78*, 184107.
[16] J. T. B. Overvelde, S. Shan, K. Bertoldi, *Adv. Mater.* **2012**.
[17] S. Janbaz, M. McGuinness, A. A. Zadpoor, *Phys. Rev. Appl.* **2018**, *9*, 064013.
[18] M. Czajkowski, C. Coulais, M. van Hecke, D. Z. Rocklin, *Nat. Commun.* **2022**, *13*, 211.

[19] Y. Zheng, I. Niloy, P. Celli, I. Tobasco, P. Plucinsky, *Phys. Rev. Lett.* **2022**, *128*, 208003.
[20] Y. Yang, K. Vella, D. P. Holmes, *Sci. Rob.* **2021**, *6*, eabd6426.
[21] Y. Hong, Y. Chi, S. Wu, Y. Li, Y. Zhu, J. Yin, *Nat. Commun.* **2022**, *13*, 530.
[22] K. K. Dudek, J. A. I. Martínez, G. Ulliac, M. Kadic, *Adv. Mater.* **2022**, *34*, 2110115.
[23] K. K. Dudek, J. A. Iglesias Martínez, G. Ulliac, L. Hirsinger, L. Wang, V. Laude, M. Kadic, *Adv. Mater.* **2023**, *35*, 2210993.
[24] S. Yan, W. Liu, X. Tan, Z. Meng, W. Luo, H. Jin, Y. Wen, J. Sun, L. Wu, J. Zhou, *Mater. Today* **2024**.
[25] H. Terrones, M. Terrones, E. Hernández, N. Grobert, J.-C. Charlier, P. M. Ajayan, *Phys. Rev. Lett.* **2000**, *84*, 1716.
[26] Y. Liu, G. Wang, Q. Huang, L. Guo, X. Chen, *Phys. Rev. Lett.* **2012**, *108*, 225505.
[27] W. McGuire, Matrix structural analysis, **2000**.
[28] H. Yasuda, Y. Miyazawa, E. G. Charalampidis, C. Chong, P. G. Kevrekidis, J. Yang, *Sci. Adv.* **2019**, *5*, eaau2835.
[29] M. Li, G. Hu, X. Chen, C.-W. Qiu, H. Chen, Z. Wang, *Sci. Adv.* **2022**, *8*, eadd6660.
[30] Z. Song, J.-F. Zhu, X. Wang, R. Zhang, P. Min, W. Cao, Y. He, J. Han, T. Wang, J. Zhu, L. Wu, C.-W. Qiu, *Nat. Commun.* **2024**, *15*, 3181.